IEEE Photonics Journal
An IEEE Photonics Society Publication

Open Access

Analysis of Cavity–Waveguide Coupling in Two-Dimensional Photonic Crystals

Volume 6, Number 3, June 2014

Ayano Tanaka
Masahiko Kondow
Masato Morifuji

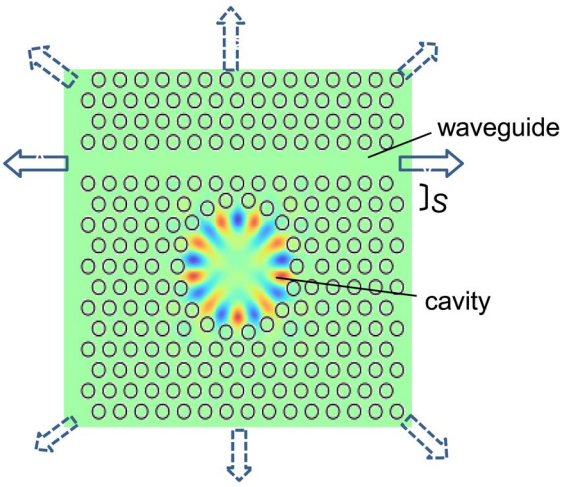

DOI: 10.1109/JPHOT.2014.2317673
1943-0655

IEEE photonics SOCIETY

IEEE

Analysis of Cavity–Waveguide Coupling in Two-Dimensional Photonic Crystals

Ayano Tanaka, Masahiko Kondow, and Masato Morifuji

Department of Quantum Electronics, Graduate School of Engineering, Osaka University, Suita, Osaka, 565-0871, Japan

DOI: 10.1109/JPHOT.2014.2317673

Manuscript received February 14, 2014; revised April 2, 2014; accepted April 4, 2014. Date of publication April 23, 2014; date of current version May 14, 2014. Corresponding author: M. Morifuji (e-mail: morifuji@eei.eng.osaka-u.ac.jp).

Abstract: We investigate theoretically cavity–waveguide coupling in 2-D photonic crystals. In using photonic crystal cavities in a device such as an optical circuit, the cavities must be coupled to a waveguide. For optimum performance, careful design of the device structure is necessary. In order to find out the rule for the design, we evaluate coupling strength by carrying out finite-difference time-domain (FDTD) calculations with systematic variation of structural parameters. Results are interpreted in terms of the density of the states of waveguide bands and symmetry of the cavity and waveguide modes. We found that the selection rule based on parity of the modes breaks down because of linewidth broadening, which arises from transition in finite time.

Index Terms: Photonic crystal, cavity mode, waveguide.

1. Introduction

Properties of nano-cavities in 2-D photonic crystals (PhCs) are attracting much interest [1], [2]. In particular, PhC lasers using the nano-cavity have been widely interested since it is a promising candidate for novel devices to be used in optical telecommunications and/or optical computing [3]–[7]. In using PhC nano-lasers in an optical circuit, connection among the nano-cavities through waveguides is necessary to transfer signals to other components in the circuit.

Light waves in a cavity–waveguide system have been widely investigated in terms of channel-drop [8], transmission spectrum [9], and slow light [10]. So far, these studies are motivated by physical interest. However, in developing optical devices using cavity–waveguide systems, careful design and fine tuning based on precise knowledge of the cavity–waveguide coupling are necessary to obtain optimum performance. If the coupling to waveguide is too strong, characteristics of the cavity will degrade. Contrary, if the coupling is too weak, the optical circuit will not work with insufficient intensity of signals. As far as we know, general rule to design a cavity–waveguide system which enables us to carry out such fine tuning of coupling strength is unknown.

In this paper, in order to find out the general design rule, we theoretically investigate the cavity–waveguide coupling. We use the finite-difference time-domain (FDTD) method to evaluate the cavity–waveguide coupling. The coupled mode theory (CMT) is also widely used for the problems of optical coupling [11]–[13]. In [11], the CMT and FDTD are compared for various cavity–waveguide structures. From the results, they conclude that FDTD is more suitable than CMT when there is a sharp resonance between cavity and waveguide. To investigate the coupling for wide variety of PhC structures, we adopted the FDTD method.

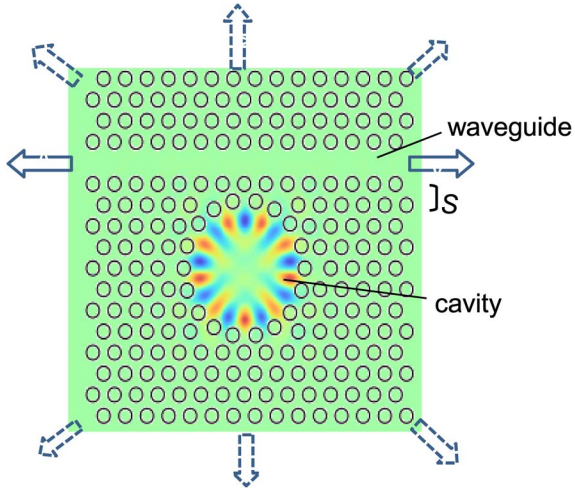

Fig. 1. A typical example of PhC structures we investigated. The PhC has a cavity resonator (modified H2 or H3) and a waveguide (W1) with separation of two rows of air holes ($S = 2$). Whispering gallery mode in the H3 cavity is also shown. The solid and dotted arrows schematically show decay of the cavity mode through the waveguide and domain border, respectively.

Fig. 1 shows an example of the PhC structures we investigated. The structure has a cavity resonator in the triangular array of air holes with the lattice constant a. We set the radius of air holes $r = 0.3a$. We considered cavities called modified H2 and H3 cavities, since a large cross section of these cavities is advantageous for an electrically-driven laser that we are developing [14]–[17]. The H2 and H3 cavities are defects with hexagonal shape consisting of seven and 19 missing air holes, respectively. We modified the cavities by shifting air holes in the periphery of the cavities so that the cavities have circular shape with radius R. Such a circular cavity generates a confined mode with high quality factor (Q-factor), called whispering gallery mode [6], [18]. A waveguide consisting of linearly aligned defects is set aside the cavity with a few rows of air holes between the cavity and waveguide. We call this a W1 waveguide.

We can tune resonance frequency of the whispering gallery mode by changing the radius R of the cavity. We can also control waveguide states by changing width of the waveguide. The number of row of the separating air holes S is also an important parameter. Changing these structural parameters systematically, we calculated coupling strength between the whispering gallery mode and waveguide mode.

2. Numerical Results and Discussion

2.1. FDTD Calculations

To evaluate strength of the cavity–waveguide coupling, we carried out FDTD calculations. Following conventional procedure of the FDTD method, we simulated temporal evolution of electromagnetic waves by solving the Maxwell's equations numerically on discretized space and time [19]. In this study, we set the mesh size of space and time as $\Delta x = a/20$ and $\Delta t = \Delta x/2c$ (c: light velocity). We used perfect matched layer for absorption boundary condition [20]. We used FullWAVE and BandSOLVE provided by the Rsoft Products to carry out FDTD simulations and photonic band calculations, respectively. First, we calculated resonance frequency of the whispering gallery mode. By using a short pulse wave source, which consists of a number of waves with different frequencies, we simulated motion of electromagnetic waves. From temporal Fourier transformation of the electromagnetic fields, we evaluated frequencies of cavity modes. Then, by using exciting wave source with one of the cavity mode frequencies, we calculated electromagnetic distribution to see if the frequency is of the whispering gallery mode. Finally, after we found the whispering gallery mode, we computed temporal change of the electromagnetic energy $U(t)$ so that

we simulate decay of the whispering gallery mode. From calculated electromagnetic energy of the cavity mode, we evaluated Q-factor by fitting $U(t)$ to an equation

$$U(t) = U(t_0)\exp(-\omega_c t/Q) \tag{1}$$

where ω_c is the frequency of the cavity mode, and t_0 is initial time.

$1/Q$ means a rate of decrease of electromagnetic energy in the cavity. If we neglect decay due to absorption, there are two types of paths for the decay of the cavity mode. One is outer border of the structure under consideration. Another is the waveguide. These paths are schematically illustrated in Fig. 1 by dotted and solid arrows, respectively. The Q-factor evaluated for the structure shown in Fig. 1 is a consequence of decay through both the paths. To extract effect of the waveguide, we additionally evaluated Q-factor for the structure without waveguide, which we denote as Q_c. Since Q_c is determined by the decay through the outer border of the system, we can define Q-factor due to decay through the waveguide by subtracting decay rate through the outer border as [13]

$$1/Q_{wg} \equiv 1/Q - 1/Q_c. \tag{2}$$

In the previous paper [21], we introduced coupling efficiency η defined by

$$\eta = \frac{1/Q_{wg}}{1/Q}. \tag{3}$$

The coupling efficiency η means a ratio of decay rate through the waveguide against the total decay rate. In this paper, however, we use Q_{wg} as a measure of the coupling strength instead of η. The reason for the use of Q_{wg} is that η depends on the system size we consider. This is because Q_c depends on the system size. This brings about a problem; if system size is very large and thus $1/Q_c$ is very small, $\eta \simeq 1$ is always satisfied. Thus, when we consider a large structure, the coupling efficiency takes the maximum value and variation of the coupling strengths among different structures is invisible. This is because, if decay through the outer border is negligibly small, cavity mode decays through only the waveguide sooner or later. As a result, $\eta \simeq 1$ is satisfied even if the coupling between cavity and waveguide is not strong. For this reason, Q_{wg} is more suitable than η as a measure of the coupling strength between cavity and waveguide. In this study, we carried out FDTD calculations for a square region $15a \times 15a$, as shown in Fig. 1.

2.2. Coupling Strength and Density of States

Fig. 2 shows $1/Q_{wg}$ calculated for the modified H3 cavities plotted as a function of waveguide width, where $2\Delta W$ denotes change in waveguide width. We note that minus sign of ΔW means decrease. We set the separation between cavity and waveguide as $S = 2$. Crosses, open circles, filled circles, and triangles are values calculated for the cavities with the radius $R = 2.76a, 2.80a$, $2.85a$, and $2.90a$, respectively. The curves have distinct peaks. In the inset, we plot normalized resonant frequencies of the cavities. Larger the cavity radius is, lower the resonant frequency shifts. Thus, the change of peak position is understood from change of resonant frequency.

In Fig. 3, we show results of photonic band calculations for the W1 waveguide obtained by using the plain wave expansion method for a 1×10 supercell. We plot dispersion curves along the Γ-X line for $\Delta W = -0.1a, 0$ and $0.1a$ from left to right. The shaded regions denote continuum band states. In the photonic band gap, there are two waveguide bands labeled mode A and mode B. These bands show higher (lower) shift with decreasing (increasing) waveguide width.

In Fig. 4(a), we plot density of states $D(\omega_c)$ at $\omega_c a/2\pi c = 0.227$ as a function of ΔW This value of ω_c is the resonant frequency of the whispering gallery mode in the $R = 2.85a$ cavity, as shown in the inset of Fig. 2. The density of states of mode n was calculated by an equation

$$D_n(\omega) = \frac{1}{\pi}\left|\frac{d\omega_n}{dk}\right|^{-1}_{\omega=\omega_n} \tag{4}$$

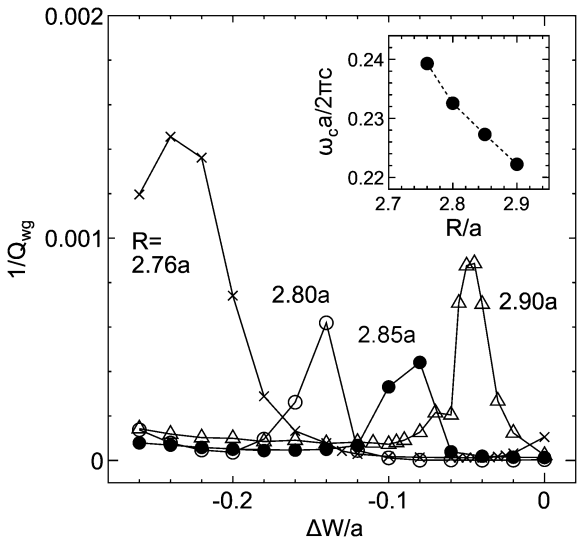

Fig. 2. $1/Q_{wg}$'s evaluated by the FDTD method for the modified H3 cavity with radius $R = 2.76a$, $2.80a, 2.85a$ and $2.90a$ are plotted as functions of decrease in waveguide width ΔW. Solid curves guide for eyes obtained by spline fitting. Inset: normalized resonant frequency ω_c is plotted as a function of cavity radius R.

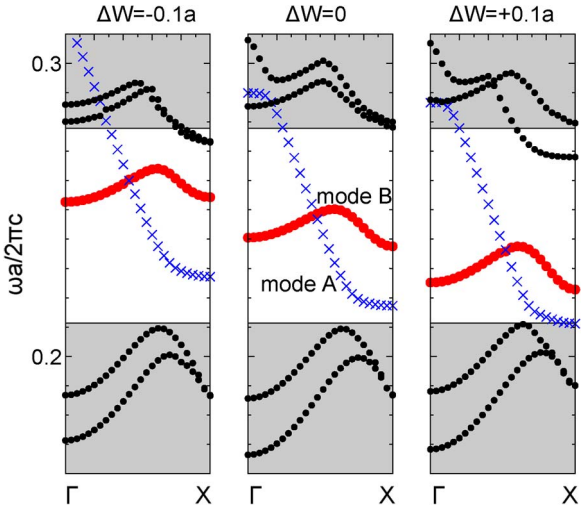

Fig. 3. Results of photonic band calculations. Dispersion curves for $\Delta W = -0.1a, 0,$ and $0.1a$ are shown. The shaded regions denote continuum band states. There are two waveguide modes labeled mode A and mode B. The waveguide bands shift to lower (higher) frequencies with decreasing (increasing) waveguide width.

with an additional broadening factor $\Delta\omega a/2\pi c = 0.002$. The crosses and filled circles denote the density of states of mode A and mode B, respectively. $D(\omega_c)$ for mode A has a peak at $\Delta W \simeq -0.08a$. $D(\omega_c)$ for mode B has peaks at $\Delta W \simeq +0.08a$ arising from the Γ and X points. As shown in Fig. 3, the waveguide bands shift toward higher frequencies with decreasing waveguide width. Since the waveguide bands have one-dimensional character, a van Hove singularity, that is, the point where inclination of the dispersion curve is nearly zero, gives rise to large density of states. As schematically shown in the inset of Fig. 4(a), density of states shifts with ΔW. When the large peak of density of states passes through ω_c, $D(\omega_c)$ becomes large. In Fig. 4(b)–(d), we show $1/Q_{wg}$ for H3 cavity with $S = 2$, H3 cavity with $S = 3$, and H2 cavity with $S = 2$. The curve of $D(\omega_c)$ is very similar to the behavior to these curves. Therefore, behavior of $1/Q_{wg}$ is well

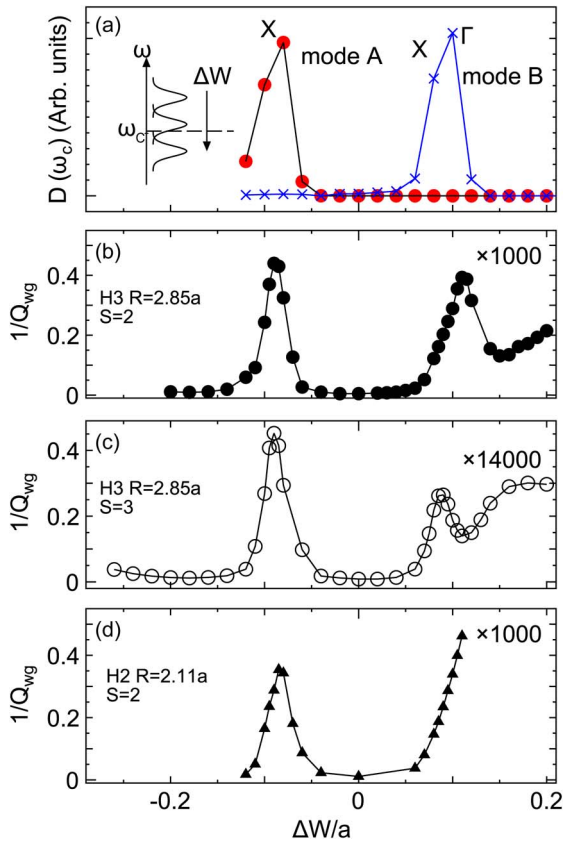

Fig. 4. (a) Density of states $D(\omega_c)$ with $\omega_c a/2\pi c = 0.227$ is plotted as a function of ΔW. (b) $1/Q_{wg}$ for the H3 cavity with $S = 2$. (c) $1/Q_{wg}$ for the H3 cavity with $S = 3$. (d) $1/Q_{wg}$ for the H2 cavity with $S = 2$.

described by change of density of states at resonant frequency of cavity mode due to shift of waveguide mode.

2.3. Mode Symmetry and Selection Rule

In Fig. 5, we show electromagnetic fields, $H_z(x, y)$, of modes relevant to the cavity–waveguide coupling. Fig. 5(a) and (b) show the whispering gallery mode in the modified H3 and H2 cavities, respectively. Among symmetries which these modes have, the mirror symmetry with respect to the y-axis is important for the coupling. We see that the whispering gallery mode in the H3 cavity is symmetric with respect to the y-axis, whereas the whispering gallery mode in the H2 cavity is anti-symmetric. Fig. 5(c)–(e) show the waveguide modes at the van Hove singularities; the X state of mode A, Γ state of mode B, and X state of mode B are shown. As is well known as a selection rule, coupling between modes with different symmetries is weak.

First, we consider the modified H3 cavity with the separation $S = 2$. Among the waveguide modes, H_z of the X state of mode A, shown in Fig. 5(c), is symmetric with respect to the y-axis indicated by the vertical dotted line. This is the same symmetry with the whispering gallery mode in the H3 cavity. As for mode B, the Γ state is symmetric, whereas the X state is anti-symmetric.

Next, we consider the modified H3 cavity with the separation $S = 3$. It should be pointed out that, when the separation S is an odd number, the dotted lines indicating the y-axis in Fig. 4(c)–(e) must be shifted by $a/2$ along the x-axis to be connected to the H3 cavity. As a result, the parities of the waveguide modes are inverted: The X state of mode A is anti-symmetric, and the X state of mode B is symmetric against the whispering gallery mode. Note that the symmetry of Γ state is unchanged due to change in separation.

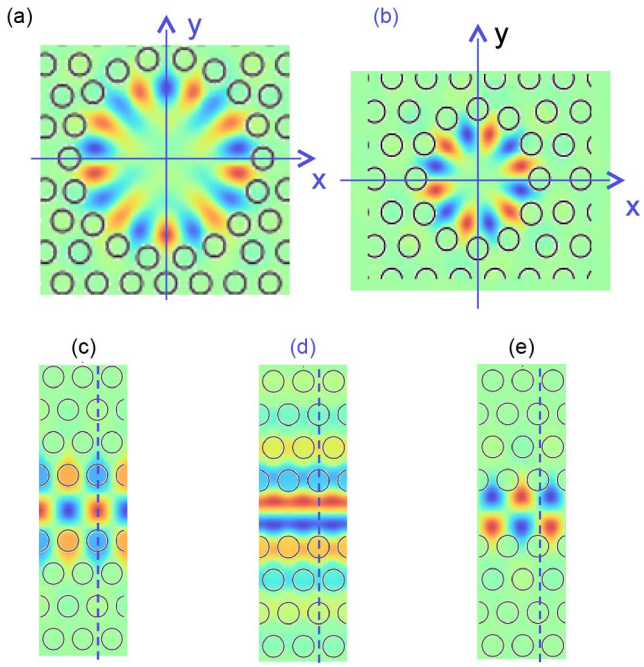

Fig. 5. Electromagnetic mode distribution $H_z(x, y)$ of modes relevant to the coupling between cavity and waveguide. The dotted line indicates the y-axis of Cartesian coordinate with the origin at the center of the cavity. Note that the dotted lines for (c)–(e) are for the case that S is an even number. When S is an odd number, the y-axis must be shifted by $a/2$.

TABLE 1

Summary of the argument on mode symmetry. The open circle and cross denote allowed and prohibited connection, respectively

	S:even		S:odd	
	H3 cavity	H2 cavity	H3 cavity	H2 cavity
mode A (X)	○	○	×	×
mode B (Γ)	○	×	○	×
mode B (X)	×	×	○	○

We can make a similar argument for the modified H2 cavity. As seen in Fig. 5(b), the whispering gallery mode in the H2 cavity is anti-symmetric with respect to the y-axis. However, compared with that for the H3 cavity, the y-axis in this case is deviated by $a/2$ along the x-axis. In accordance with this shift of the y-axis, the y-axis (dotted lines) in Fig. 5(c)–(e) also must be shifted by $a/2$ to be connected with the H2 cavity. As a result, the X state of mode A becomes anti-symmetric, and the X state of mode B is symmetric with respect to the deviated y-axis. Since both the cavity mode and waveguide modes change the symmetry, the same selection rule as H3 cavity with $S = 2$ is satisfied. We summarize the selection rule in Table 1, where allowed and prohibited couplings are shown by the open circles and crosses, respectively.

Let us look back results shown in Fig. 4(b)–(d) from view point of mode symmetry. In Fig. 4(b), the peak at $\Delta W \simeq -0.08a$ is understood as transition between the cavity mode and waveguide mode A(X) because combination of these modes results in allowed transition. The peak at $\Delta W \simeq 0.08a$ in Fig. 4(b) is also reasonably understood, considering that the cavity mode can connect with the Γ state of mode B. In Fig. 4(c), the peak at $\Delta W \simeq 0.08a$ appears slightly lower position compared with that in Fig. 4(b). This is a result of symmetry change mentioned above; For $S = 3$, cavity mode connects not the Γ state but the X state. These results show that mode symmetry has a certain role in the cavity–waveguide coupling. However, the peak at $\Delta W \simeq -0.08a$ in Fig. 4(c) is arising from prohibited connection. The peak at $\Delta W \simeq -0.08a$ in Fig. 4(d) is also prohibited. We may expect that these peaks do not appear or are smaller than others.

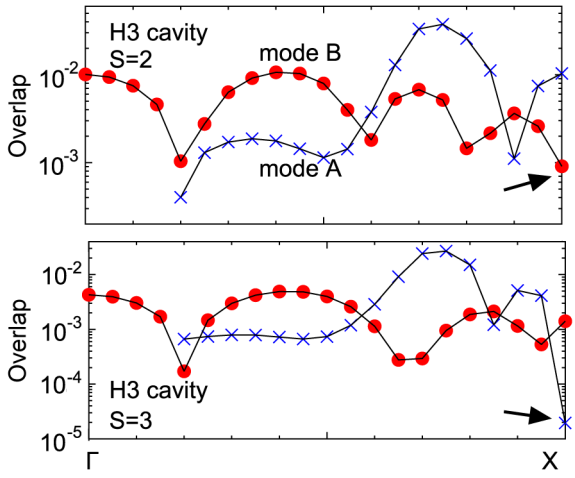

Fig. 6. Absolute value of overlap between the whispering gallery mode and waveguide mode along the Γ-X line. Crosses and filled circles denote the overlap for mode A and mode B, respectively. Arrows show prohibited coupling.

To explain this contradiction, we calculated overlap between the whispering gallery mode and waveguide mode defined by

$$O = \frac{\left\langle H_z^{wg} | H_z^{cavity} \right\rangle}{\sqrt{\left\langle H_z^{wg} | H_z^{wg} \right\rangle \left\langle H_z^{cavity} | H_z^{cavity} \right\rangle}} \tag{5}$$

where $\langle \cdots \rangle$ denotes intagral. Results are shown in Fig. 6 where arrows show prohibited coupling. As indicated by arrow, the overlap between H3 and X state of mode A for $S = 3$ is very small. However, since the overlap strongly depends on wavevector, the overlap has large value at k-points near the X. Since transition from cavity to waveguide is a phenomenon within a finite time scale, linewidth broadening arises from the uncertainty principle. As a result, many states near the X point are involved in the coupling. Even if the coupling to the X state is prohibited, the states in vicinity bring about coupling. For this reason, the curves in Fig. 4(c) and (d) have a peak at $\Delta W = -0.08a$, even though the coupling is prohibited by the selection rule.

For the problems of optical coupling between cavities or between cavity and waveguide, the coupled mode theory (CMT) is widely used. The CMT provides useful theoretical framework and physical insight for the problem. CMT calculations are often carried out with overlap integrals only at symmetry points. Therefore, in the present situation where a number of waveguide states are involved, CMT calculations could be tedious to obtain the same results as FDTD. As we have noted, the overlap integral strongly depends on wavevector of the waveguide states. It is not easy to carry out the CMT calculations in the present situation because a large number of overlap integrals between the cavity state and the waveguide states are necessary.

In order to clarify the role of the broadening, we calculated coupling strength for the H3 cavity with $S = 3$ using an equation known as the Fermi's golden rule

$$1/Q_{wg}^F \equiv \frac{a}{\pi} \int_{\Omega} |O_k|^2 dk = a \int_{\omega_c - \Delta\omega/2}^{\omega_c + \Delta\omega/2} |O_\omega|^2 D(\omega) d\omega \tag{6}$$

where O_k (or O_ω) is the overlap integral. Considering the broadening, upper and lower limit of ω-integration (or corresponding region of k-summation Ω) is $\omega_c \pm \Delta\omega/2$. In Fig. 7, we show $1/Q_{wg}^F$ calculated for the H3 cavity with the separation $S = 3$. using (6) with $\Delta\omega a/2\pi c = 0.01, 0.004$,

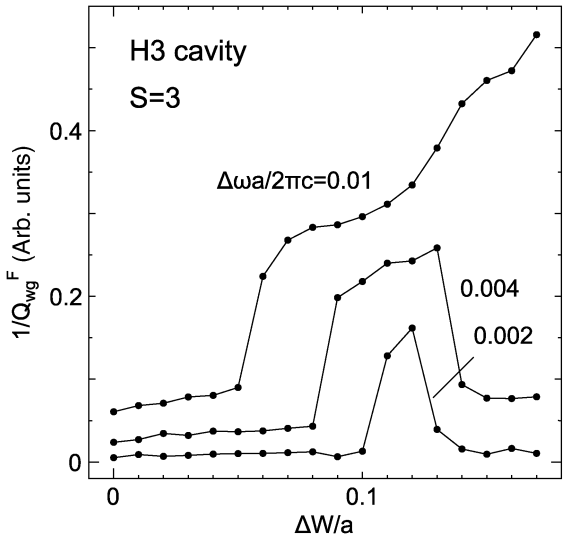

Fig. 7. $1/Q_{wg}^{F}$ evaluated by using Fermi's golden rule for H3 cavity with $S = 3$.

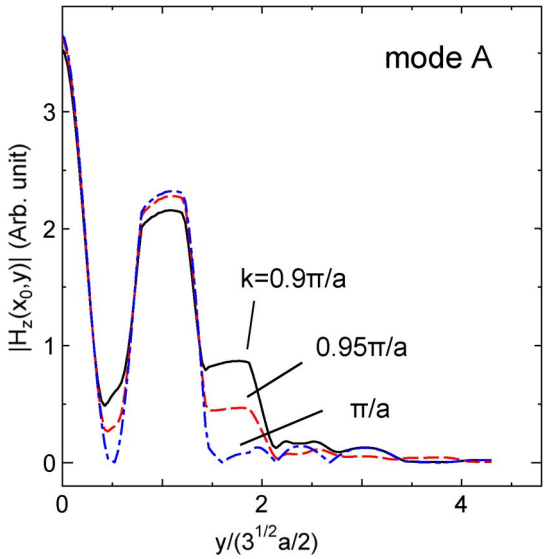

Fig. 8. $|H_z(x_0, y)|$ of mode A for $k = 0.9\text{X}, 0.95\text{X},$ and X along the y-axis by solid, dashed, and dot-dashed curves, respectively.

and 0.002. Since this is corresponding to the result shown in Fig. 4(c), comparing the curves in Figs. 4(c) and 7, we see that $\Delta\omega a/2\pi c$ is about 0.002.

Broadening in frequency $\Delta\omega$ is also estimated from Δt the time for light to reach the waveguide as $\Delta\omega \simeq 1/\Delta t$. From FDTD calculations, we evaluated that $\Delta t \simeq 10 \times \Delta y/(c/n)$ where Δy is distance between the cavity and waveguide and n is refractive index. Considering that $\Delta y/a$ is $2 \sim 3$, we have roughly $\Delta\omega a/2\pi c \simeq 0.002$. This value agrees well with the result estimated from the Fermi's golden rule.

Finally, in Fig. 8, we plot $|H_z(x_0, y)|$ of mode A along the y-axis with x_0 a position where the modes have antinode. Solid, dashed, and dot-dashed curves denote the state for $k = 0.9\text{X}$, 0.95X, and X, respectively. We see that the modes at $k = 0.9\text{X}$ and 0.95X have large amplitude at $y \simeq \sqrt{3}a$ where outskirt of the cavity mode locates. We also note that these k-points are within the region of broadened X state. This is corresponding well to the wavevector dependence of overlap of mode A near the X point shown in lower panel of Fig. 6.

3. Conclusion

For the purpose of obtaining rules to design a cavity–waveguide system in a two dimensional photonic crystal, we carried out FDTD calculations and evaluated strength of the coupling with systematic variation of structure such as cavity radius and waveguide width.

Since cavity–waveguide coupling strongly depends on density of states of waveguide mode, the coupling becomes strong when resonant frequency of cavity mode and van Hove singularity are close in frequency.

The W1 waveguide has two waveguide bands, which we refer mode A and mode B. Mode A has the van Hove singularity at the X point. Mode B has three van Hove singularities at the Γ, X, and an intermediate point.

The optical coupling also depends on symmetry of the cavity and waveguide modes. However, simple selection rule based on the parity of the modes does not hold. This is because that overlap between the modes strongly depends on wavevector of the waveguide state. Since transition between cavity and waveguide is a temporal phenomenon, many waveguide states are involved. Therefore, the selection rule is smeared out.

References

[1] E. Yablonovitch, "Inhibited spontaneous emission in solid-state physics and electronics," *Phys. Rev. Lett.*, vol. 58, no. 20, pp. 2059–2062, May 1987.

[2] S. John, "Strong localization of photons in certain disordered dielectric super lattices," *Phys. Rev. Lett.*, vol. 58, no. 23, pp. 2486–2489, Jun. 1987.

[3] S. Matsuo *et al.,* "High-speed ultracompact buried heterostructure photonic-crystal laser with 13 fJ of energy consumed per bit transmitted," *Nature Photon.*, vol. 4, no. 9, pp. 648–654, 2010.

[4] S. Matsuo *et al.,* "20-Gbit/s directly modulated photonic crystal nanocavity laser with ultra-low power consumption," *Opt. Exp.*, vol. 19, no. 3, pp. 2242–2250, Jan. 2011.

[5] L. Chen and E. Towe, "Design of high-Q microcavities for proposed two-dimensional electrically pumped photonic crystal lasers," *IEEE J. Sel. Topics Quantum Electron.*, vol. 12, no. 1, pp. 117–123, Jan./Feb. 2006.

[6] M. Morifuji, Y. Nakaya, T. Mitamura, and M. Kondow, "Novel design of current driven photonic crystal laser diode," *IEEE Photon. Tech. Lett.*, vol. 21, no. 8, pp. 513–515, Apr. 2009.

[7] M. Morifuji and Y. Nakaya, "Numerical design of photonic crystal cavity structure with AlAs/AlOx cladding layers for current-driven laser diodes," *Jpn. J. Appl. Phys.*, vol. 48, no. 11, p. 112001, 2009.

[8] S. Fan, P. R. Villeneuve, J. D. Joannopoulos, and H. A. Haus, "Channel drop filters in photonic crystals," *Opt. Exp.*, vol. 3, no. 1, pp. 4–11, Jul. 1998.

[9] S. Fan, "Sharp asymmetric line shapes in side-coupled waveguide-cavity systems," *Appl. Phys. Lett.*, vol. 80, no. 6, pp. 908–910, Feb. 2002.

[10] Y. Lu, X.-H. Huang, X.-Y. Fu, D.-P. Chu, and J.-Q. Yao, "Theoretical study on modulating group velocity of light in photonic crystal coupled cavity optical waveguide," *Optoelectron. Lett.*, vol. 8, no. 1, pp. 25–28, Jan. 2012.

[11] N. Avaritsiotis, T. Kamalakis, and T. Sphicopoulos, "On the effectiveness of coupled mode theory in the analysis of photonic crystal coupled resonator devices," *J. Lightw. Technol.*, vol. 29, no. 5, pp. 736–743, Mar. 2011.

[12] E. Waks and J. Vuckovic, "Coupled mode theory for photonic crystal cavity-waveguide interaction," *Opt. Exp.*, vol. 13, no. 13, pp. 5064–5073, Jun. 2005.

[13] A. Schwagmann *et al.,* "In-plane single-photon emission from a L3 cavity coupled to a photonic crystal waveguide," *Opt. Exp.*, vol. 20, no. 27, pp. 28614–28624, Dec. 2012.

[14] Y. Kitabayashi, M. Mochizuki, F. Ishikawa, and M. Kondow, "Over 1.5 μm deep dry etching of Al-rich AlGaAs for photonic crystal fabrication," *Jpn. J. Appl. Phys.*, vol. 52, no. 4S, p. 04CG07, 2013.

[15] S. Yamauchi, M. Morifuji, and M. Kondow, "Fabrication and analysis of current confinement structure for photonic crystal laser," *Physica Status Solidi (c)*, vol. 10, no. 11, pp. 1465–1468, Nov. 2013.

[16] T. Okabe, M. Morifuji, and M. Kondow, "Role of aluminum oxide cladding layers in heat transfer in a semiconductor slab with photonic crystal," *Jpn. J. Appl. Phys.*, vol. 53, no. 2, pp. 022701-1–022701-6, 2014.

[17] R. Nakao and M. Morifuji, "Effects of carriers on characteristics of current-driven photonic crystal laser diode," *Jpn. J. Appl. Phys.*, vol. 52, no. 1R, p. 012002, 2013.

[18] S. G. Johnson, S. Fan, A. Mekis, and J. D. Joannopoulos, "Multipole-cancellation mechanism for high-Q cavities in the absence of a complete photonic band gap," *Appl. Phys. Lett.*, vol. 78, no. 22, pp. 3388–3390, May 2001.

[19] A. Taflove and S. C. Hagness, *Computational Electrodynamics.* Boston, MA, USA: Artech House, 2005.

[20] J.-P. Berenger, "A perfect matched layer for the absorption of electromagnetic waves," *J. Comp. Phys.*, vol. 114, no. 2, pp. 185–200, Oct. 1994.

[21] K. Nagahara, M. Morifuji, and M. Kondow, "Optical coupling between a cavity mode and a waveguide in a two-dimensional photonic crystal," *Photon. Nanostructures—Fundam. Appl.*, vol. 9, no. 3, pp. 261–268, Jul. 2011.

[22] P. Chak, S. Pereira, and J. E. Sipe, "Coupled-mode theory for periodic side-coupled microcavity and photonic crystal structures," *Phys. Rev. B*, vol. 73, no. 3, p. 035105, 2006.

[23] M. Loncar, T. Doll, J. Vuckovic, and A. Scherer, "Design and fabrication of silicon photonic crystal optical waveguides," *J. Lightw. Technol.*, vol. 18, no. 10, pp. 1402–1411, Oct. 2000.